FINE STRUCTURE IN A METRIC TYPE IV BURST: MULTI-SITE SPECTROGRAPHIC, POLARIMETRIC, AND HELIOGRAPHIC OBSERVATIONS

G. P. CHERNOV
IZMIRAN, 142092 Troitsk, Moscow Region, Russia

K.-L. KLEIN
DASOP, CNRS-URA 1756, Observatoire de Paris, Section d'Astrophysique de Meudon, 92195 Meudon, France

P. ZLOBEC,
Osservatorio Astronomico, via G.B. Tiepolo 11, 34131 Trieste, Italy

and

H. AURASS
Astrophysikalisches Institut Potsdam, Observatorium für solare Radioastronomie, 14552 Tremsdorf, Germany

(Received 20 December, 1993; in revised form 10 August, 1994)

Abstract. The spectral fine structure of solar radio continua is thought to reveal wave-particle and wave-wave interactions in magnetic traps in the solar corona. We present observations of spectra, polarization, and spatial characteristics of combined emission/extinction features ('zebra patterns') during a decimetric/metric type IV event on 5 June, 1990. Very high modulation depths are observed. The size and location of the sources during emission and extinction are determined for the first time. Two remarkable features are found: (1) The sources of emission stripes have finite size, up to nearly 2′; during extinction stripes the brightness is reduced across the whole extent of the unperturbed continuum, which is slightly larger than 2′. (2) During emission stripes the sources drift over distances up to several $\times 10^4$ km, with apparent velocities up to 10^5 km s^{-1}. The observed features are briefly discussed with respect to interpretations based on wave-particle interactions and on the scattering of electromagnetic waves.

1. Introduction

Particles accelerated during flares are partly injected into closed coronal structures where they become trapped. Such configurations likely give place to various instabilities whereby waves are generated, such as Langmuir waves and whistlers, which subsequently interact with the trapped particles and may change the trapping conditions. Various types of fine structure identified in dynamic spectra of decimetric and metric continuum emission ('type IV') have been ascribed to wave-wave and wave-particle interactions in coronal traps (Kuijpers, 1975; Bernold, 1980; Slottje, 1981; Aurass *et al.*, 1987). Among them are drifting bands of combined emission and extinction features. The latter are called *fiber bursts* or *intermediate drift bursts* when consisting of a single band with nearly constant drift rate, and *zebra pattern* when composed of several simultaneous bands with often a time-variable drift rate.

Solar Physics **155:** 373–390, 1994.

Fiber bursts are generally explained by the coupling of Langmuir waves (l) with whistlers (w), $l + w \rightarrow t$ (Kuijpers, 1975; Mann, Karlický, and Motschmann, 1987). A widely accepted interpretation of zebra patterns, however, has not yet emerged. They were originally ascribed to be the growth of upper hybrid waves at frequencies where the upper hybrid frequency, ω_{uh}, is a multiple of the cyclotron frequency, ω_{ce}, of the electrons (double plasma resonance):

$$\omega_{uh} = \sqrt{\omega_{pe}^2 + \omega_{ce}^2} = N\omega_{ce} \,, \tag{1}$$

where $N = 2, 3, \ldots$, and ω_{pe} is the electron plasma frequency. Theories based on this mechanism were proposed by Kuijpers (1975), Zheleznyakov and Zlotnik (1975), Berney and Benz (1978), Mollwo (1983, 1988), Winglee and Dulk (1986), and reviewed by Kuijpers (1980). The occurrence of emission and extinction stripes in both zebra lines and fiber bursts motivates their interpretation in the framework of a unique mechanism. Therefore Chernov (1976, 1990a, b) proposed that zebra lines are generated by whistler wave packets propagating obliquely to the magnetic field, and fiber bursts by whistlers ducted in overdense coronal structures. Thus, zebra stripes are produced when a whistler trajectory intersects a region where the electrons emitting the type IV continuum are trapped.

So far, observations of fiber bursts and zebra patterns have been discussed using dynamic spectra of flux density, and sometimes polarization, without spatial resolution. A statistical study was carried out by Slottje (1981). A detailed analysis of individual events is found, e.g., in Slottje (1972), Chernov, Korolev, and Markeev (1975), Kuijpers, van der Post, and Slottje (1981), Aurass and Chernov (1983). Imaging observations can improve the understanding of spectral fine structures: on the one hand they constrain the association of fine structure features with other types of activity, such as flares or filament eruptions, as well as the magnetic topology of the plasma-magnetic-field configuration near the site of emission. On the other hand they should display details of the source configuration, such as the relative position of sources of continuum and fine structure, which may give deeper insight into the relevant plasma processes. The present paper reports on radio observations which combine for the first time spectrographic, polarimetric, and imaging diagnostics. The observations are presented in Section 2, starting with a brief description of the instruments (Section 2.1). An overview of the active region and of the evolution and structure of the radio sources is given in Section 2.2. Selected fine structures are presented in Section 2.3 with emphasis on the temporal evolution of their flux density spectrum, as well as the position and size of the radio sources during different phases of emission/extinction features.

TABLE I
Characteristics of the radio instruments

Name	Frequencies (MHz)	Type of observations
IZMIRAN Moscow	90–180, 180–270	Swept freq. spectrom., sweep rate 50 Hz, freq. resol. 0.2 MHz
	169, 204	Total flux density, time res. 1 s
OSRA Tremsdorf	100–164	Swept freq. spectrom., sweep rate 10 Hz
	30, 60, 80, 112, 136, 160, 234 775, 140, 2000, 3000, 9500	Total flux density, partly circ. pol. time res. 62 ms
Trieste Radio Polarimeter	237, 327, 408, 610	Total flux density and circ. polar., time res. 20 ms
Nançay Radioheliograph (NRH)		1D scans in total (I) and circ. polar. intensity (V)
East–west array	164	time res. 50 ms, Beam (FWHM)=1.2′
North–south array	164, 236.6, 327, 408, 435	time res. 0.25 s, Beam (FWHM)= 3.2′ × 164 MHz/ν

2. Observations

2.1. Instruments

The observations were carried out jointly with instruments providing spectrally and spatially resolved data including circular polarization. The characteristics of the instruments are listed in Table I.

2.2. Overview of the structure and activity of AR 6086

The radio event of interest occurred from 09:35 to 11:50 UT on 5 June, 1990, in AR NOAA 6086. Figure 1 (left panel) shows the Ca II K_{1v} spectroheliogram taken at Meudon at 11:20 UT. The active region 6086 was located at N22° E08°. It had a simple structure, classified β between 1 and 4 June, 1990, and α by all but one observatory on 5 June (*Solar Geophysical Data* 552, I). Prior to the event of interest a noise storm was observed at metric and decametric wavelengths. Its sources are overlaid upon the Ca photograph in Figure 1. The cross gives the position of the centroid and the half width of the source as measured with the east–west and the north–south arrays of the NRH at 164 MHz. The straight lines represent the one-dimensional location determined by the north–south array at 236.6 MHz (solid), 327 (short dashes, nearly the same as the 236.6 MHz position) and 408 MHz (long dashes).

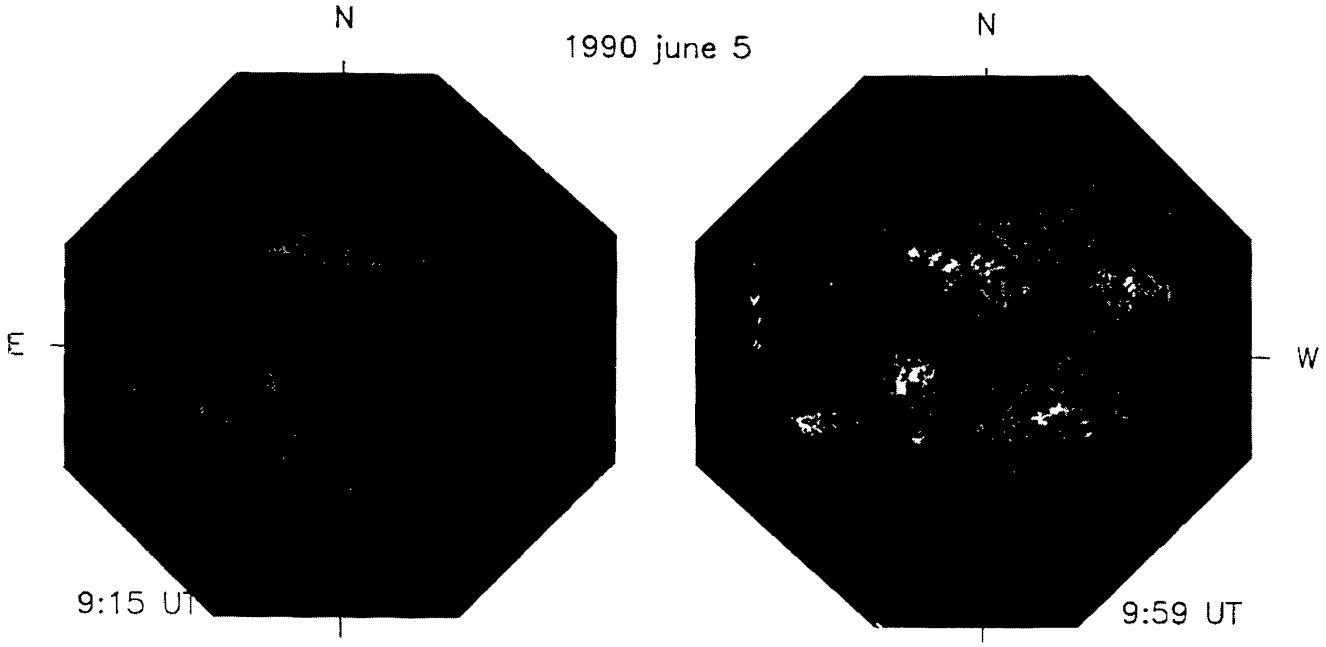

Fig. 1. Images of the Sun at optical wavelengths (Meudon spectroheliograph) and radio positions (Nançay Radioheliograph, NRH) on 5 June, 1990. Solar north is at the top, east on the left. The crosses give the position and half widths of the sources measured with the east–west and north–south arrays of the NRH at 164 MHz, straight lines the one-dimensional positions at 236.6 (solid), 327 (short dashes), and 408 MHz (long dashes) determined by the north–south array. *Left*: positions of the noise storm at 09:15 UT are overlaid upon the Ca II K_{1v} photograph of the Sun at 11:20 UT. *Right*: the two sources during the type IV burst at 09:59 UT are overlaid upon the Hα photograph taken at 07:05 UT. Most of the subsequent type IV emisson comes from the southern source.

Between 09:35 and 11:50 UT bright, strongly polarized emission is observed mainly at meter wavelengths (327–30 MHz, Figure 2). Towards short wavelengths the emission is cut off near 2 GHz. The spectrum, polarization and time history are typical of a noise storm enhancement or storm continuum (e.g., Kai, Melrose, and Suzuki, 1985; Pick, 1986). The fluctuations of the radio emission consist mostly of rapid fine structure with larger bandwidth than type I bursts. The radio event will therefore be referred to as a type IV burst in the following. At metric and decimetric wavelengths the emission comes from two sources. The configuration at 09:59 UT is overlaid upon the Meudon Hα spectroheliogram (taken at 07:05 UT) in the right panel of Figure 1. The southern source is by far the brightest. Since the one-dimensional positions are the same at all frequencies observed by the NRH, the sources are likely located in magnetic structures directed towards an active region in the southern hemisphere (0.5 $R_\odot$ south of AR 6086, cf. Figure 1).

At all observed frequencies where polarization measurements are available, both the continuum and the fine structure are totally right-hand circularly polarized (as is the preceding noise storm). Comparison of the radio positions with photospheric magnetograms suggests that the dominant radio source is connected to a region of

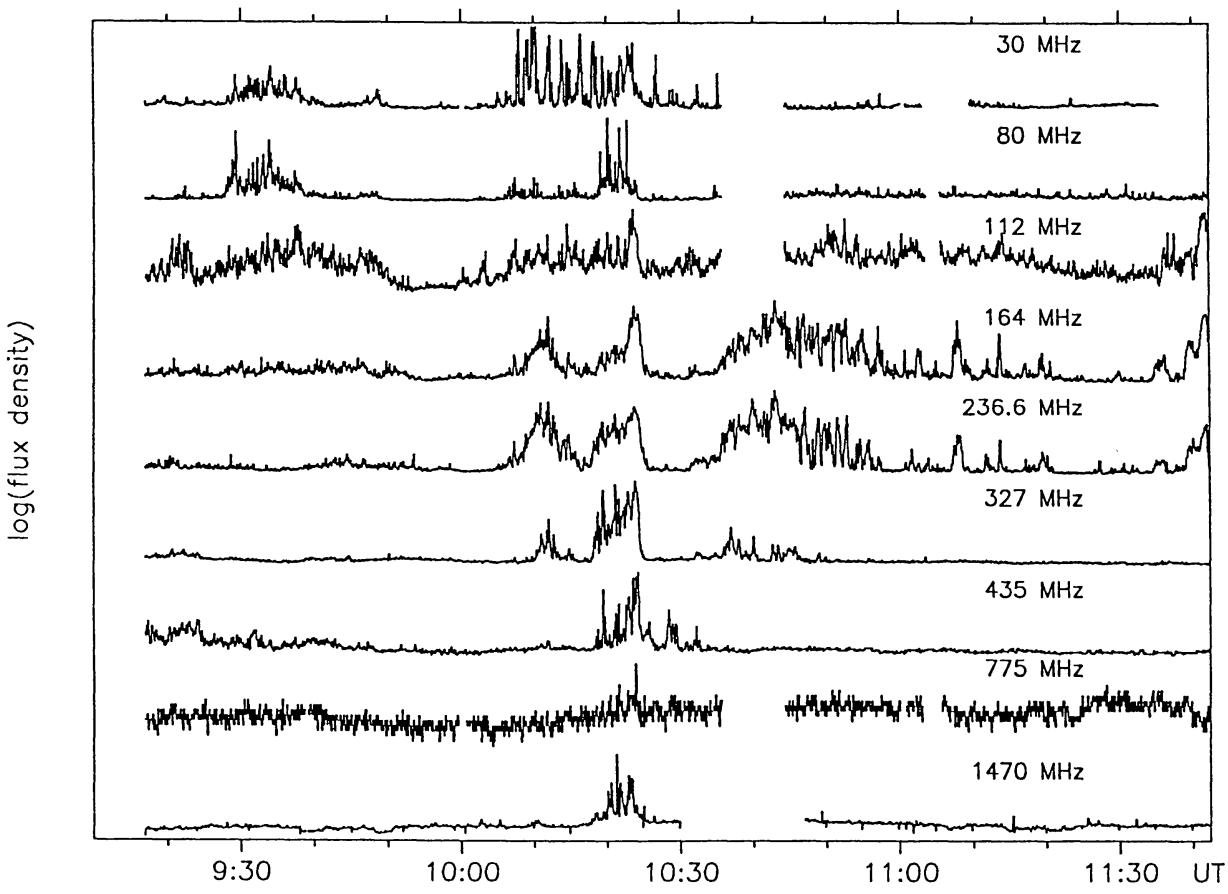

Fig. 2. Time history of the radio emission from decametric (*top*) to decimetric (*bottom*) wavelengths (OSRA Tremsdorf: 30–112, 775, 1470 MHz; NRH: 164–435 MHz). The scale is linear at 1470 MHz, logarithmic at the other frequencies. The emission is composed, from 09:35 to 11:50 UT, of a continuum, mainly in the range 30–327 MHz. The high-frequency cutoff of the continuum is around 2 GHz.

southern magnetic polarity within AR 6086. The radio emission is thus likely in the ordinary mode.

The Hα spectroheliogram shows that filaments surround the active region in a semi-circle from east over north to west. The smaller filament inside this semi-circle changed its shape between 4 and 5 June (07:05 UT) and was not seen any more at 12:54 UT (Sacramento Peak Hα photograph, *SGD* 552, I). Close to the brightening of the radio emission at 09:35 UT the soft X-ray flux starts a smooth rise to a maximum of GOES class B8 (at 11 UT), while the only Hα flare reported on 5 June, 1990 from AR 6086 starts nearly one hour after the radio brightening; a faint subflare from 10:49 to 11:03 UT. It therefore appears that the radio type IV event is related with a slowly evolving soft X-ray brightening, possibly with a filament activation and eventual eruption, but is not initiated by a conspicuous flare.

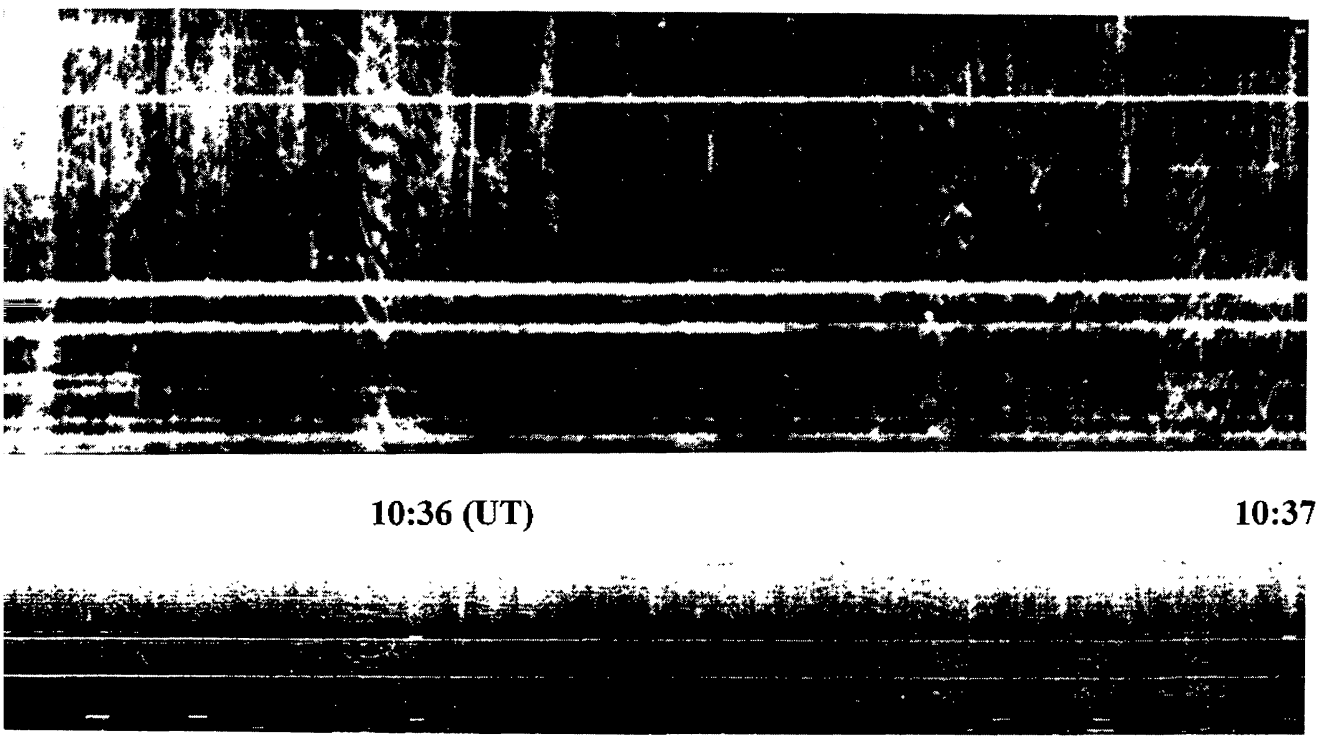

Fig. 3. Dynamic spectra during the type IV event on 5 June, 1990 as observed in the same frequency range by two widely separated spectrographs (OSRA Tremsdorf, *top*; IZMIRAN Troitsk, *bottom*). The frequency increases from top to bottom. The flux density is shaded from black (low flux density) to white. The narrow horizontal lines are due to terrestrial interference. The same fine structures are observed with both instruments. Conspicuous zebra patterns with rapidly changing frequency drift occur shortly before 10:36 UT and between 10:36:30 and 10:37 UT.

2.3. Selected Fine Structures of the Type IV Burst

Figure 3 compares dynamic spectra of the flux density taken at OSRA Tremsdorf and at IZMIRAN. The same fine structure features are seen with both instruments, whose sites are separated by about 2000 km. This demonstrates the solar origin of the spectral structure. It consists of zebra patterns with multiple stripes of emission (white) and extinction (black), e.g., shortly before 10:36 UT and between 10:36:30 and 10:37 UT.

Figure 4 shows a section of the early phase of the event, displaying broadband pulsations (10:20:45 to 10:20:50 UT), zebra stripes (10:21:00 to 10:21:03 UT) and an enhancement of the continuum emission (10:21:07 to 10:21:15 UT): dynamic spectrum between 226 and 260 MHz, single-frequency record of total flux density at 237 MHz, and contour plot of the one-dimensional (relative) brightness as a function of position and time at 236.6 MHz. The position of the brightest point in

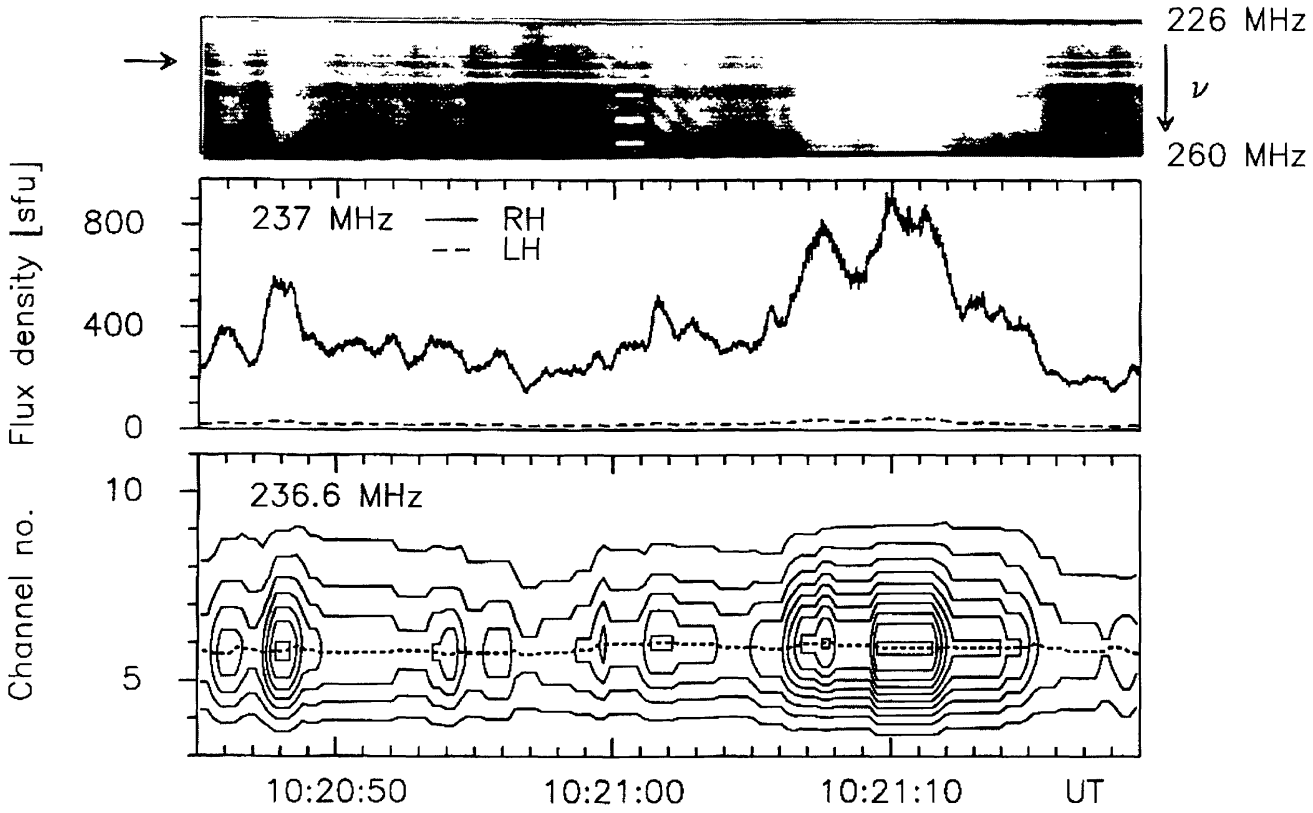

Fig. 4. Different spectral features in the band 226–260 MHz occurring during the type IV event on 5 June, 1990: broadband pulsations (10:20:46–10:20:56 UT), zebra stripes (10:20:00–10:21:04 UT) and the peak of the more slowly varying continuum emission (10:21:06–10:21:15 UT). From top to bottom: (1) Dynamic spectrum (IZMIRAN, the horizontal arrow points to 237 MHz); (2) flux density at 237 MHz (Trieste) in left-hand (dashed) and right-hand (solid) polarization; (3) contour plots of the relative brightness at 236.6 MHz (NRH, north–south array). The contours go from 9 to 99% of the highest intensity value in the plotted field, in steps of 10%. The dashed line through the centre of the highest contour gives the position of peak brightness. The vertical axis is graded in units of 1.4′, from terrestrial south to north. The projected position of the centre of the solar disk is in channel 0.

the one-dimensional brightness distribution is marked by the dashed line through the centre of the highest contours. The prolonged horizontal sections of the contours (e.g., from 10:20:50 to 10:20:52 UT) are a consequence of the data compression where subsequent scans whose difference does not exceed a given amount, are considered identical (Radioheliograph Group, 1989). The contours are asymmetric, due to the weak secondary source $\sim 3'$ north of the main emission. The fine structure sources are embedded in the continuum at the southern position of Figure 1, but small displacements are discernible between the brightness maxima during different spectral features:

(1) The source centroid is located at the same (one-dimensional!) position during the phases of zebra lines (channel 5.93 ± 0.06, 10:21:00–10:21:05 UT) and continuum emission (channel 5.92 ± 0.04, 10:21:07–10:21:11 UT).

(2) The average position of the brightest emission during the earlier interval 10:20:44 to 10:20:57 UT, including the broadband pulsations, is in channel 5.77 ± 0.06.

The average values and standard deviations were derived exclusively from the non-compressed scans. The projected distance between the source centroids during pulsations and of the continuum source amounts to $13'' \pm 7''$. Since the transition between the two positions occurs within a few seconds, coinciding with the change of the spectral structure, the shift is not an instrumental or ionospheric effect.

In the following we focus on the combined features of emission and extinction during the type IV event. We present first the spectral observations and then the evolution of positions and sizes of the radio sources.

2.3.1. *Spectrographic Observations of Zebra Stripes*

In the dynamic spectrum of Figure 5, zebra stripes with opposite frequency drift are seen between 10:45:20 and 10:45:25 UT. In this case the positively drifting stripes are similar to fiber bursts, consisting of emission stripes with constant frequency drift, accompanied by low-frequency extinctions (see Slottje, 1981). The stripes are best visible as extinction of the continuum at frequencies below roughly 240 MHz, and as emission on a background of weak continuum at higher frequencies. Altogether they form a sequence of emission and extinction throughout the frequency range covered. As this feature drifts towards higher frequencies, it crosses oppositely drifting stripes. When an emission ridge from one set intersects an extinction stripe from another set, the emission stripes are strongly reduced. The process by which the continuum is extinguished therefore also reduces the emission stripe. This can only occur if the emission and extinction stripe are generated in the same volume.

The extinction may be very pronounced: at 10:45:21 UT (Figure 5) the modulation at 237 MHz, defined as

$$m = \frac{I_{\max} - I_{\min}}{I_{\max} + I_{\min}}\,, \tag{2}$$

where I, denoting the whole-Sun flux density, is about 90%. It never attains 100% and varies with time (gradual decrease from 66 to 27% in the series of zebra lines at 10:45:27.5 UT, Figure 5; gradual increase from 20% to 40%, 10:37:52 and 10:37:56 UT). Near the end of the event a series of zebra stripes is observed in emission (Figure 6), with increasing modulation depth.

The sets of stripes displayed in Figure 5 form a remarkably regular pattern, where the sense of frequency drift changes, e.g., at 10:45:22, 10:45:25.5, and 10:45:40 UT. The pattern suggests that the individual sets are not independent.

2.3.2. *Shifts of Source Positions*

The evolution of the one-dimensional source position at 236.6 MHz (NRH) is plotted at the bottom of Figure 5. Given the integration time of 0.25 s, the rapid

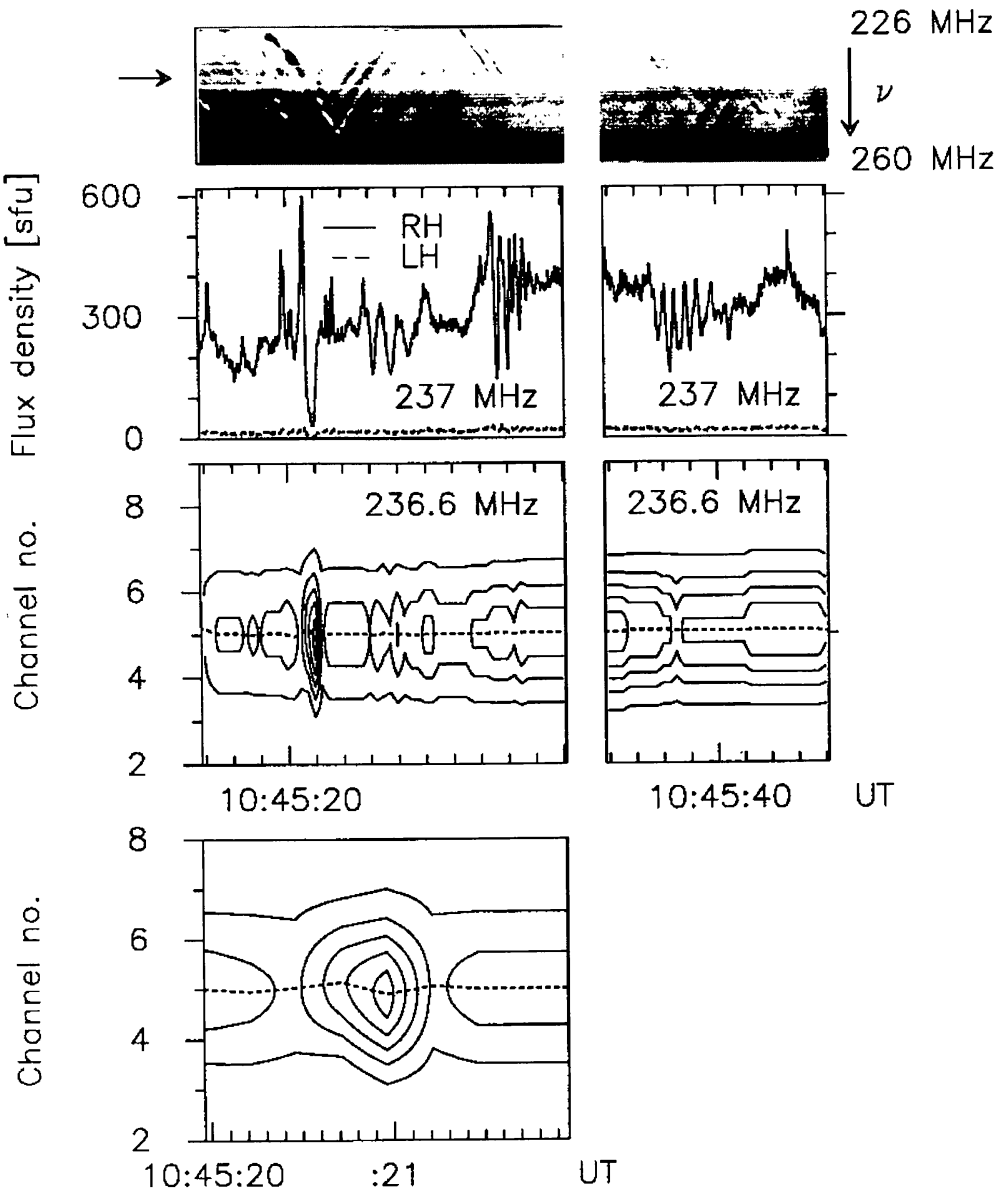

Fig. 5. Section with oppositely drifting zebra stripes. The two top panels give the dynamic spectrum and the 237 MHz record of the flux density. The abscissa is graded in steps of 1 s. Two spectral features are remarkable: (1) Crossing zebra stripes, 10:45:20–10:45:24 UT: the positively (downward) drifting emission stripe is extinguished as it intersects the negatively (upward) drifting extinction stripe at 10:45:22 UT near the high-frequency edge of the spectrum. (2) Modulation depth of zebra stripes: systematic decrease from 66% to 27%. The third row from the top gives the evolution of brightness and source position at 236.6 MHz (NRH) as in Figure 4, with contours from 9 to 89% of the biggest intensity, in steps of 20%. The fourth panel shows a zoom on the combined emission/extinction stripe at 10:45:21 UT.

variations seen in the Trieste data (e.g., 10:45:27 to 10:45:29 UT) are smeared out, and the data are heavily compressed, such that the extinction feature at 10:45:20 UT is barely visible. The centroid of the continuum source, plotted by the dashed line through the centre of the highest contour, is stable during the 13-s interval shown (3rd row from top). On the other hand, during the zebra stripe at 10:45:20 UT the

centroid undergoes an oscillating drift: northward at the onset of the stripe, then back to the former continuum position where the brightest emission during the stripe occurs, and again northward during the fading of the stripe (bottom panel). The positional difference is 0.2 channels, i.e., about 17″.

The displacement is clearer in Figure 6, where zebra stripes appear in emission (superimposed on a weak continuum, which is visible in the 237 MHz records). The position of maximum brightness is again seen to drift from the rising to the fading phase of the stripes. The shift starts with a northward displacement at the onset of the stripe, followed by a monotonic southward drift during 0.5 s, throughout the rise and decrease of the brightening. The monotonic displacement is not generated by the brightening of an independent source near the continuum, but reveals the systematic shift of the emitting region during the emission stripe. During the most prominent case at 11:27:14.5 UT (bottom panel) the drift covers 0.56 channels (47″). The velocity component along the terrestrial north–south baseline is about 7×10^4 km s^{-1}. During the following stripes more irregular motions, as at 10:45:21 UT, are again observed.

In order to check the accuracy of the position measurements, we computed the scattering of the positions of maximum brightness during the time interval of Figure 5, using only those data points which are not affected by compression, and excluding the interval around the zebra stripe at 10:45:21 UT. This yields an r.m.s. variation around the mean value of 0.025 channels (2″). The position changes detected during the zebra stripes are therefore significant.

Due to the limited temporal resolution of the NRH north–south array we cannot describe the time history of the displacement better at 236.6 MHz. Both the contours and the lines of maximum brightness in the bottom panel of Figures 5 and 6 are interpolated between individual measurements with 0.25 s integration. Therefore the preceding discussion is based on three measured points during the emission stripe. Similar shifts of emission throughout the rise and decay of intensity are, however, also visible at 164 MHz with the east–west array (50 ms resolution). For example, during the interval of zebra stripes shown in Figure 7 the centroid of the source starts at a position east of the preceding continuum, drifts towards the former continuum position which is attained during the maximum brightness of the emission stripe, and continues the westward drift until the fading of the emission stripe. Then a new cycle starts east of the continuum source. The sense of the drift motion is the same, irrespective of the sense of the spectral drift of these zebra stripes. The total distance covered by the drift is of the order of 2×10^4 km, and the projected velocity $\approx 10^5$ km s^{-1}.

It is concluded that definite evidence for the displacement of the radio source of emission stripes is given by the imaging observations. Their detailed aspect may vary between individual stripes, and cases without detectable shift are also frequently found in the data.

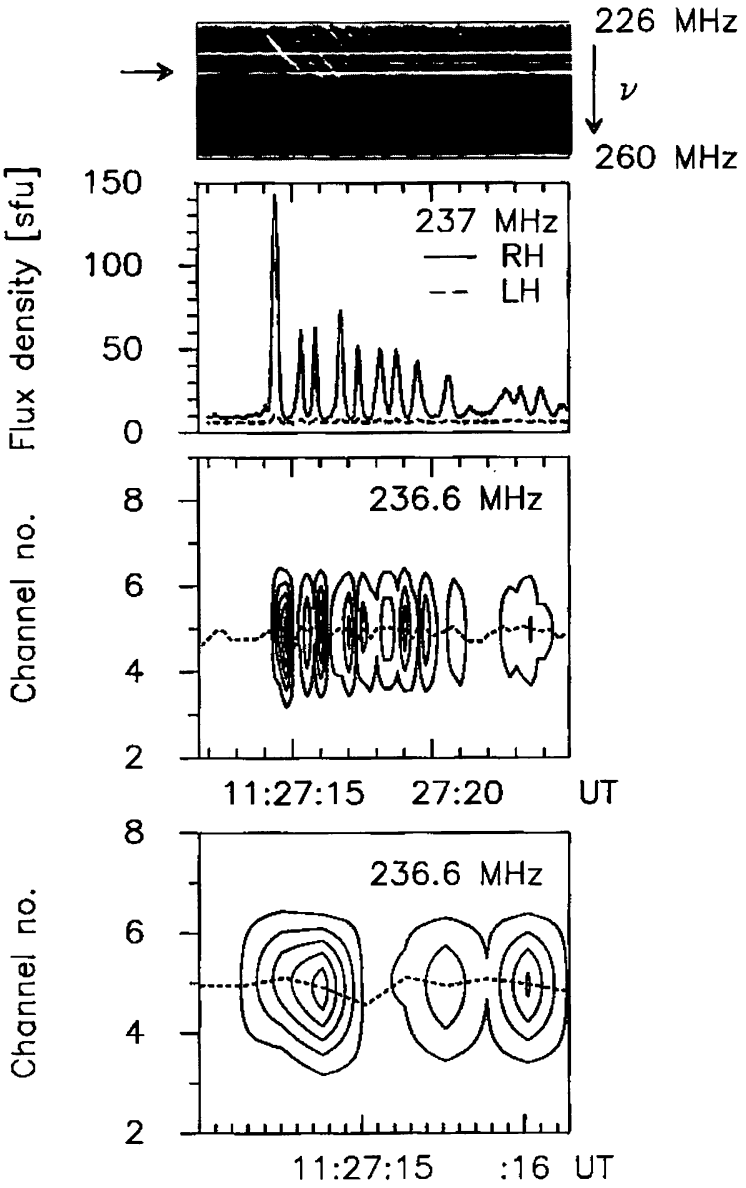

Fig. 6. Series of zebra stripes in emission near the end of the type IV event. From *top to bottom*: dynamic spectrum, 237 MHz flux density in left- (dashed) and right-hand (solid) polarization; 1D map at 236.6 MHz together with the position of maximum brightness; zoom on the first zebra stripes. In the NRH records significant emission is found throughout the plotted time interval, as indicated by the line that delineates the position of maximum brightness. The oscillation of this position near 11:27:12.5 UT occurs during a short emission feature which is too weak to be identified in the dynamic spectrum.

2.3.3. Source Structure and Dimensions during Zebra Patterns

Inspection of the angular dimensions during the different periods of zebra fine structure around 237 MHz shows that none of the sources is point-like. One cannot exclude the possibility that several distinct sources contribute within one integration period of 0.25 s. We therefore consider the 50 ms observations at 164 MHz with the east–west array of the NRH. One-dimensional scans are displayed in Fig-

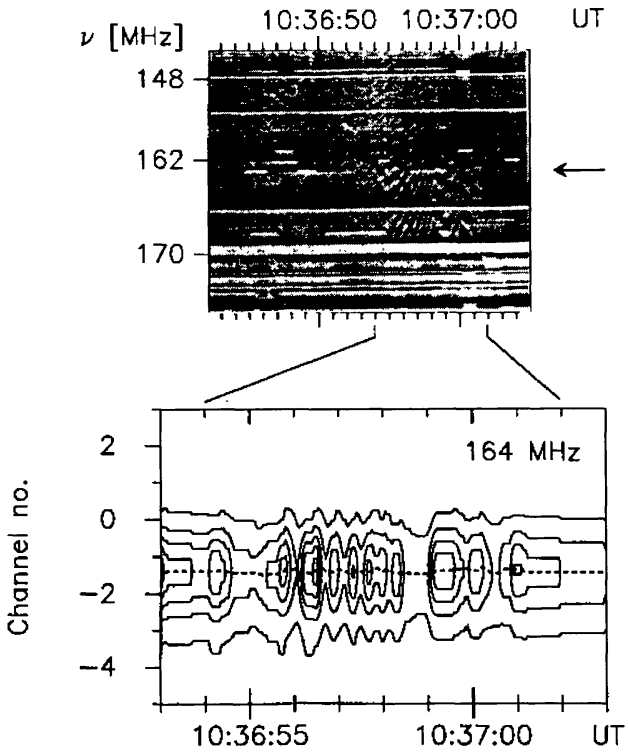

Fig. 7. Temporal evolution of the dynamic spectrum and source position during an interval of zebra pattern activity near 164 MHz. Dynamic spectrum (IZMIRAN; the horizontal arrow on the right indicates 164 MHz); 1D map at 164 MHz together with the position of maximum brightness (NRH, east–west array; 1 channel $\approx 1.0'$).

ure 8(a) for three features prior to and during the zebra pattern of Figure 7: the unperturbed continuum before the zebra stripes (10:36:53.50 UT, long dashes), an emission stripe (10:36:56.45 UT, short dashes) and the subsequent extinction stripe (10:36:56.70 UT, solid line). The sources are structureless, and no qualitative difference is apparent between them. The basic distinguishing feature is the brightness, which is reduced in the whole source of unperturbed continuum emission during the extinction stripe and enhanced during the emission stripe. Figure 8(b) shows the time history of the peak brightness (top) and of the size (bottom) of the emitting source. The size is understood as the half-power width of the Gaussian fit to the undeconvolved source, and is expressed as a multiple of the beam of the NRH. The vertical lines show the instants of the source profiles plotted in Figure 8(a). Throughout the zebra pattern 10:36:53 to 10:37:03 UT the measured angular size is greater than that of a point source, which would have diameter 1 in this plot. Besides by direct measurement, this is also shown by the weak level of sidelobes in the profiles (Figure 8(a)). Near the brightest phase of the zebra stripes, the source width is 1.5–1.6 times the beam. At this size the broadening by the beam is weak. The measured half width is $1.9'$ ($0.1\ R_\odot$), and gives a brightness temperature of roughly 10^{10} K (for a circular source) during the brightest peak at 10:36:56.45 UT.

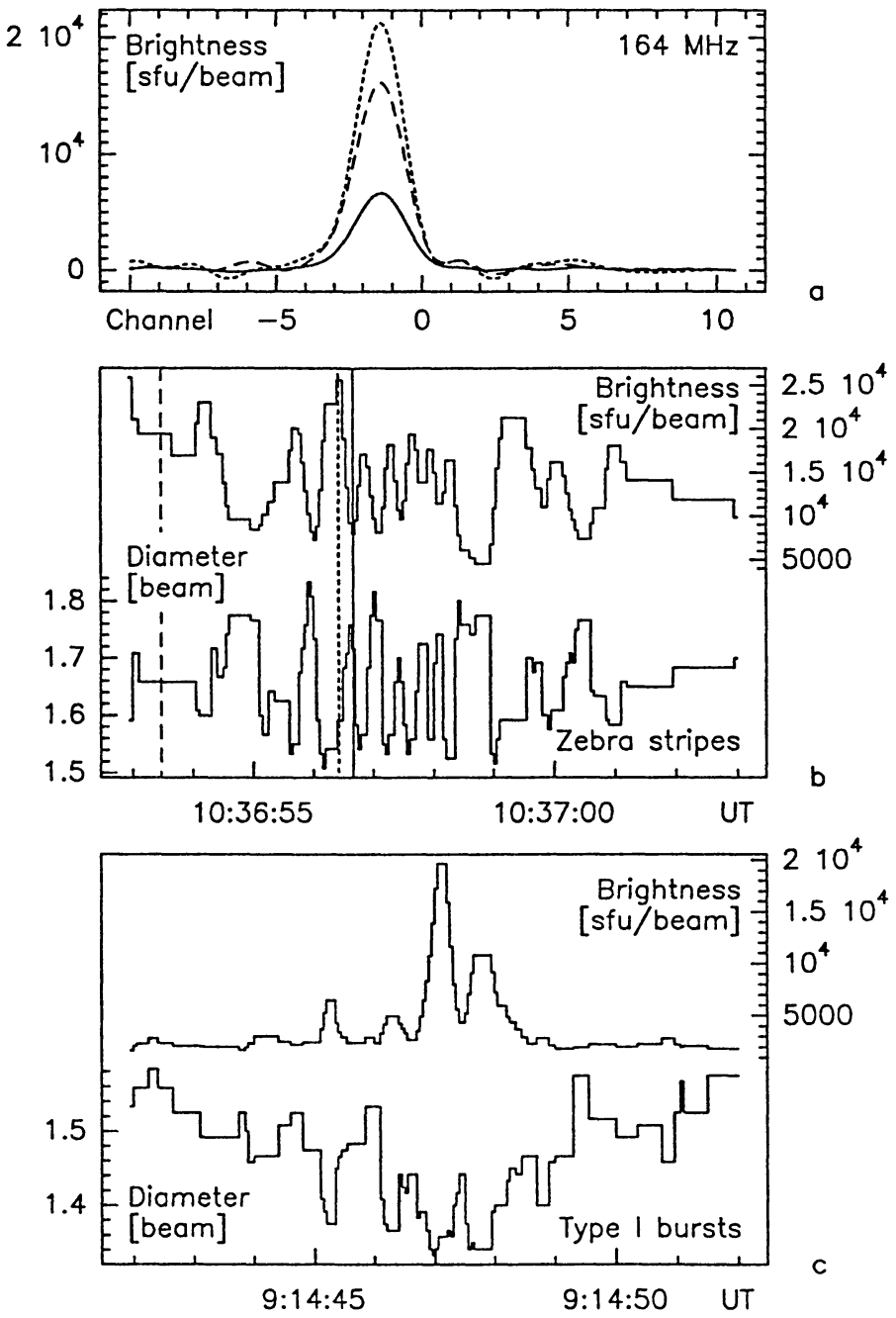

Fig. 8. Temporal evolution of the 164 MHz emission during the interval of zebra pattern activity of Figure 7. (a) One-dimensional brightness distributions with 50 ms integration time during the unperturbed continuum (10:36:53.50 UT, long dashes), an emission stripe (10:36:56.45 UT, short dashes) and the subsequent extinction stripe (10:36:56.70, solid line). (b) Time history of the brightness (*top*) and half-power diameter (*bottom*) during the zebra pattern. (c) Time history of brightness and diameter of type I bursts during the noise storm preceding the type IV event. The brightness and diameter in (b) and (c) are those of a Gaussian fit to the observed source profiles.

During the phases of extinction and of the unperturbed continuum emission the source appears slightly broader, typically 2.1′ and 2.0′, respectively.

For comparison, Figure 8(c) shows the peak brightness and source dimension during a section of the noise storm which preceded the type IV event. The time interval includes two type I bursts at 09:14:47 and 09:14:48 UT. The source of the type I bursts is also not point-like ($\sim$ 1.3 times the beam), as was already known from former observations (Kerdraon, 1973). Due to Earth rotation, the beam of the east–west array of the NRH narrows from 1.4′ at 09:15 to 1.2″ at 10:37 UT. The source sizes of the zebra emission stripe and the type I bursts are therefore comparable.

3. Summary and Discussion

Combining instruments with high spectral, temporal and spatial resolution, we have observed a bright decimetric-to-metric continuum, which comprises different types of spectral fine structure with characteristic times <1 s. Imaging observations are used for the first time to analyse combined emission/extinction features of dm/m-wave continua.

The event is not clearly associated with an Hα flare, but is probably closely connected with the activation and destabilization of a filament in a simple active region. The observations are summarized as follows:

(1) The sources of type IV continuum and fine structure are located in a coronal configuration which is globally stable during nearly 2 hours.

(2) The position of the radio source suggests that it is connected with a region of southern magnetic polarity in the photosphere. The polarization of the radio source then implies emission in the ordinary mode.

(3) Different types of fine structure (fast pulsations, zebra pattern) come from different locations within a great magnetic structure. The observed separations are of the order of ten to some tens of arc seconds. This is smaller than the diameter of the continuum source.

(4) The continuum is strongly modulated by zebra stripes in emission and extinction (up to 90%). But even during extinction a remnant of the continuum is seen, both in the total solar flux densities and in the imaging data.

(5) The extinction stripe does not only reduce the continuum, but also the emission stripe in cases where zebra stripes with opposite drift cross each other.

(6) The sources of zebra stripes in emission are not point-like. Sizes up to 1.9′ are observed. During the extinction stripes, slightly larger sources are seen ($\approx$ 2.1′). These sizes are close to those of the unperturbed continuum.

(7) Apparent displacements of the emitting sources are observed during many zebra stripes. These displacements may either be monotonic from the rise through the maximum and the decline of an emitting feature, or change direction around the time of maximum brightness. The observed shifts range up to several tens of arc sec, i.e., several 10^4 km, between the onset and the end of an emission ridge, corresponding to apparent velocities up to 10^5 km s^{-1}. There is no qualitative

difference between the positional shifts during positively and negatively drifting stripes.

In the following we briefly discuss these observations in terms of the interaction of Langmuir waves with whistlers and of the double resonance model. We also comment on the possible role of scattering and refraction of electromagnetic waves in broadening and shifting the source images.

3.1. Spectral features during zebra patterns

The key features of the dynamic spectrum reported in this paper are:

– the crossing of zebra stripes with opposite drift,

– the strong modulation of the continuum by zebra stripes in emission and extinction.

Crossing zebra stripes are not a mere coincidence of features from independent sources superposed in the spectrum due to the lack of spatial resolution. This is proved especially by the extinction of the positively drifting emission stripe at the time when it crosses the negatively drifting extinction stripe (10:45:22 UT). In the framework of the theory of Langmuir wave-whistler interaction, the crossing stripes are attributed to the crossing of two whistler trajectories. The oppositely drifting features hence show that different (at least two) sites of instabilities exist from which perturbations propagate in opposite directions, or else that a propagating disturbance is reflected. In the latter case the succession of stripes with changing senses of frequency drift between 10:45:20 and 10:45:40 UT would suggest multiple reflections of the exciting agent.

The reported event displays a wide variety of modulation depths. Features with similar temporal, polarimetric, and heliographic properties are seen either as a combination of emission and extinction ridges superposed upon a continuum emission or as emitting features with only weak (but significant) underlying continuum emission. If extinction features are superposed upon a continuum, the modulation depth varies with time. Modulation depths as high as 90% were detected in this event, which are higher than reported in previous work (Aurass and Chernov, 1983). The extinction must therefore operate on the whole continuum source at a given frequency. In the framework of the Langmuir wave-whistler model the amount of extinction depends on the quasi-linear diffusion process, which can be more or less efficient depending on the energy density of the whistlers.

3.2. Spatial characteristics of different types of sources during zebra patterns

The source of the zebra stripes is extended, similar to a type I source in the pre-existing noise storm. Taking together the finite receiver bandwidth, the finite height range occupied by the whistler wave packet (Chernov, 1976) and its finite bandwidth due to velocity dispersion of the fast electrons which generate the whistlers, a height extent of several 10^8 cm is expected for the emitting volume in

the whistler-Langmuir-wave model. On the other hand, theory does not provide a stringent limit on the *lateral* extent of the whistler wave packet.

Frequently shifts of the position occurred throughout the rise and decay of zebra stripes. Velocities of up to 10^5 km s^{-1} were inferred, similar to those identified by Trottet *et al.* (1981) in pulsations of type IV emission. While drifts of the source position can qualitatively be explained, e.g., by spatial variations of the Langmuir wave intensity across the emitting volume due to spatial variations of the electron distributions which generate the waves (cf. Figures 4 to 6 of Chernov, 1978), the observed scales ranged up to several tens of arc seconds. They were hence also bigger than the estimated height-extent of the emitting volume, but smaller than the observed source size. The inferred velocities are higher than expected for whistler waves. Hence, while the effect can be qualitatively understood in terms of a propagating exciter, the big distances and high velocities observed suggest that the origin of the shifts is not yet satisfactorily explained.

In the double resonance model the region of zebra stripe emission is given by the resonance condition (1), which describes a surface of nearly arbitrary extent. The allowed magnetic field variation across the observed source is given by the receiver bandwidth $\Delta\omega$:

$$\frac{\Delta B}{B} = \frac{\Delta\omega_{ce}}{\omega_{ce}} = \frac{\Delta\omega}{\omega} \approx 3.5 \times 10^{-3}$$

(cf. Table I). Such a small variation requires nearly identical surfaces of equal field strength and equal density over the observed source size ($\approx 10^5$ km), hence a very smooth density variation. It cannot be excluded that this is the case, but it is not likely to be so in a low-β plasma such as the solar corona.

Nearly (but not fully) aligned surfaces of constant B and constant n_e also provide favourable conditions for rapid source motion at a fixed frequency, because a small magnetic field change implies a significant shift of the intersection between ω_{uh} and $N\omega_{ce}$ in order to satisfy Equation (1) within the receiver bandwidth. In this case one would expect to see different directions of positional shift corresponding to different senses of frequency drift of the zebra stripes. This was not observed in the zebra stripes with rapidly changing sense of frequency drift (Figures 5 and 7).

As an alternative to both models, the radioheliographic observations can also be discussed in terms of electromagnetic wave propagation effects in the corona. For example, scattering has been cited as a means to broaden intrinsically small radio sources in order to explain the finite dimensions of type I bursts (Kerdraon, 1973, 1979; Elgarøy, 1977; Zlobec *et al.*, 1992). In this view zebra emission sources would be considered as intrinsically point-like. If the emission and extinction during a zebra pattern are due to the same agent, such as whistlers which couple with Langmuir waves to yield an electromagnetic wave (emission) and isotropize the electron distribution which generates the Langmuir waves (extinction), the undisturbed continuum source must be point-like, too. The size of metric continuum sources has been discussed in the case of noise storms. Most theories

consider that the source is intrinsically large, and interpret the continuum as the spontaneous emission of Langmuir waves (e.g., Melrose, 1980; Benz and Wentzel, 1981; Wentzel, 1986). The identical spectrum and circular polarization suggest that type IV continua of the kind discussed in this paper are of similar nature as noise storm continua. If type IV continua turn out to be emitted by point-sources, the ideas on noise storm continua will have to be reconsidered, too.

Source motions can also be generated by scattering or refraction of electromagnetic waves (cf., e.g., the review by Rickett (1990) on wave propagation in the interstellar medium). We have recently observed apparent motions similar to those discussed here during a fundamental type II burst at 164 MHz. Since the spectral fine structure in this type II burst (and during the pulsations reported by Trottet *et al.*, 1981) is not reminiscent of the zebra pattern, while the common property of the radio bursts is emission at the plasma frequency, propagation effects which are independent of the type of radio emission might explain the similar apparent source motions.

We conclude that the interpretation of the observations is an open problem in both classes of zebra-stripe theories. Since the sources of zebra fine structure reveal spatial complexity on scales accessible to the presently available angular resolution, the combination of radio spectrography, polarimetry, and imaging must be developed in future systematic studies.

Acknowledgements

The authors are indebted to Drs A. Kerdraon, J. Kuijpers, and G. Trottet for helpful comments on the manuscript. G.C. is grateful for the support by Paris Observatory and the Italian Research Council (CNR) that enabled him to work with colleagues at Meudon and Trieste, respectively. Part of his research was made possible by grant No. Ph1–1513–0924 from the International Science Foundation and the Russian Founding of Fundamental Investigation. P.Z. acknowledges support of CNR, the Italian Ministry for University and Research (MURST) and the Consorzio di Magnetofluidodinamica of the Trieste University. Work at Paris Observatory was supported by CNRS.

References

Aurass, H. and Chernov, G. P.: 1983, *Solar Phys.* **84**, 339.
Aurass, H., Chernov, G. P., Karlický, M., Kurths, J., and Mann, G.: 1987, *Solar Phys.* **112**, 347.
Benz, A. O. and Wentzel, D. G.: 1981, *Astron. Astrophys.* **94**, 100.
Berney, M. and Benz, A. O.: 1978, *Astron. Astrophys.* **65**, 369.
Bernold, T.: 1980, *Astron. Astrophys. Suppl. Series* **42**, 43.
Chernov, G. P.: 1976, *Soviet Astron.* **20**, 582.
Chernov, G. P.: 1978, *Soviet Astron.* **22**, 330.
Chernov, G. P.: 1990a, *Soviet Astron.* **33**, 649.
Chernov, G. P.: 1990b, *Solar Phys.* **130**, 75.
Chernov, G. P., Korolev, O. S., and Markeev, A. K.: 1975, *Solar Phys.* **44**, 435.

Elgarøy, Ø: 1977, *Solar Noise Storms*, Pergamon Press, Oxford.
Kai, K., Melrose, D. B., and Suzuki, S: 1985, in D. J. McLean and N. R. Labrum (eds.), *Solar Radiophysics*, Cambridge University Press, Cambridge, p. 145.
Kerdraon, A.: 1973, *Astron. Astrophys.* **27**, 361.
Kerdraon, A.: 1979, *Astron. Astrophys.* **71**, 266.
Kuijpers, J.: 1975, 'Collective Wave-Particle Interactions in Solar Type IV Radio Sources', Thesis, Utrecht University.
Kuijpers, J.: 1980, in M. R. Kundu and T. E. Gergely (eds.), 'Radio Physics of the Sun', *IAU Symp.* **86**, 341.
Kuijpers, J., van der Post, P., and Slottje, C.: 1981, *Astron. Astrophys.* **103**, 331.
Mann, G., Karlický, M., and Motschmann, U.: 1987, *Solar Phys.* **110**, 381.
Melrose, D. B.: 1980, *Solar Phys.* **67**, 357.
Mollwo, L.: 1983, *Solar Phys.* **83**, 305.
Mollwo, L.: 1988, *Solar Phys.* **116**, 323.
Pick, M.: 1986, *Solar Phys.* **104**, 19.
Radioheliograph Group: 1989, *Solar Phys.* **120**, 193.
Rickett, B. J.: 1990, *Ann. Rev. Astron. Astrophys.* **28**, 561.
Slottje, C.: 1972, *Solar Phys.* **25**, 210.
Slottje, C.: 1981, *Atlas of Fine Structures of Dynamic Spectra of Solar Type IV-dm and Some Type II Radio Bursts*, Utrecht Observatory.
Trottet, G., Kerdraon, A., Benz, A. O., and Treumann, R.: 1981, *Astron. Astrophys.* **93**, 129.
Wentzel, D. G.: 1986, *Solar Phys.* **103**, 141.
Winglee, R. M. and Dulk, G. A.: 1986, *Astrophys. J.* **307**, 808.
Zheleznyakov, V. V. and Zlotnik, E. Ya.: 1975, *Solar Phys.* **44**, 461.
Zlobec, P., Messerotti, M., Dulk, G. A., and Kucera, T.: 1992, *Solar Phys.* **141**, 165.